A new heat transfer fluid for concentrating solar systems: Particle flow in tubes

Gilles Flamant, Daniel Gauthier, Hadrien Benoit, Jean-Louis Sans, Benjamin Boissière, Renaud Ansart, Mehrdji Hemati

A new heat transfer fluid for concentrating solar systems: Particle flow in tubes

G. Flamant[a]*, D. Gauthier[a], H. Benoit[a], J.-L. Sans[a], B. Boissière[b], R. Ansart[b], M. Hemati[b]

[a]*Processes, Materials and Solar Energy laboratory, PROMES-CNRS, 7 rue du Four Solaire, Font Romeu, France*
[b]*Université de Toulouse; INPT, UPS; LGC (UMR-CNRS 5503) 4 Allée Émile Monso BP 84234 31432 Toulouse Cedex 4, France*

Abstract

This paper demonstrates a new concept of heat transfer fluid (HTF) for CSP applications, developed in the frame of both a National and a European project (CSP2 FP7 project). It involves a dense suspension of small solid particles. This innovation is currently. The dense suspension of particles receiver (DSPR) consists in creating the upward circulation of a dense suspension of particles (solid fraction in the range 30%-40%) in vertical absorbing tubes submitted to concentrated solar energy. So the suspension acts as a heat transfer fluid with a heat capacity similar to a liquid HTF but only limited in temperature by the working temperature limit of the receiver tubes. Suspension temperatures up to 750°C are expected for metallic tubes, thus opening new opportunities for high efficiency thermodynamic cycles such as supercritical steam and carbon dioxide.

First experimental results were obtained during on-sun testing with CNRS solar facility of a single tube DSPR for an outlet temperature lower than 300°C. In this lab-scale experimental setup, the solar absorber is a single opaque metallic tube, containing upward solid circulation, located inside a cylindrical cavity dug in a receiver made of refractory, and submitted to the concentrated solar radiation through a 0.10m x 0.50m slot. The absorber is a 42.4 mm o.d. stainless steel tube. SiC was used because of its thermal properties, availability and rather low cost. The 63.9 μm particle mean diameter permits a good fluidization with almost no bubbles, for very low air velocities.

Solar flux densities in the range 200-250 kW/m^2 were tested resulting in solid temperature increase ranging between 50 and 150°C. The mean wall-to-suspension heat transfer coefficient (h) was calculated from experimental data. It is very sensitive to the solid fraction of the solid suspension, which was varied from 27% to 36%. These latter values are one order of magnitude larger than the solid fraction in circulating fluidized beds operating at much higher air velocity. Heat transfer coefficients ranging from 140 to 500 W/m^2.K have been obtained; i.e. 400 W/m^2.K mean value for standard operating conditions at low temperature.

doi:10.1016/j.egypro.2014.03.067

Keywords: dense suspension of solid particles ; fluidization ; central solar receiver ; heat transfer fluid ; heat transfer coefficient

1. Introduction

Concentrated solar systems may produce high temperature heat and power efficiently and firmly thanks to heat storage and hybridization. Among available technologies, solar tower (or central receiver system) offers numerous options for producing heat at temperature higher than 500°C, temperatures that are needed to power efficient Rankine thermodynamic cycles. In solar tower, sun-tracking heliostats reflect solar radiation to the top of a tower where is located the receiver (solar absorber). In the receiver, solar heat is transferred to a heat transfer fluid (HTF). The HTF transports the heat to the energy conversion sub-system that includes a heat storage, heat exchangers, an optional burner for fuel back-up and a power block. Industrially, current HTF are steam and nitrate salts, air (at atmospheric pressure and pressurized) is under development. These existing HTF have drawbacks, in particular limited working temperature domain for salt (typically 240-565°C for binary sodium-potassium nitrate salt), very high pressure for steam and poor heat transfer capacity for air. A solution to overcome these drawbacks is using solid particles as HTF.

Solid particles (silica sand, bauxite or silicon carbide for example) may be used as heat transfer fluid in solar thermal concentrating systems in direct heating and indirect heating receivers. In the former case solid particles absorb directly the concentrated solar radiation, and in the latter case a heat transfer wall is used, the wall absorbs solar radiation and transfers the heat to a flowing heat transfer medium. In particular tubular absorbers are mainly used in current solar thermal power plants. Solid particle solar receivers associated with solar tower concentrating systems offer very interesting options for high temperature and high efficiency power cycles, thermal storage integration (using the same particles as HTF and storage medium) and chemical applications of concentrated solar energy (thermo-chemical water splitting process to produce hydrogen, cement processing, for example).

First studies on direct absorption solar receivers started in the early 1980s with two concepts, the fluidized bed receiver [1] and the free falling particles receiver [2]. In the first concept the solid particles are fluidized in a transparent tube but do not flow outside, there is no solid circulation. Consequently the system was used to heat air or to process reactive particles in batch operation [3]. In the free falling particles curtain concept, the solid is dropped directly into the concentrated solar beam from the top of the receiver and is heated during the passage time through the irradiated part of the receiver tube. Particle selection and radiative heat transfer modeling have been proposed [4,5].

After about twenty years without new development, this concept was again proposed as a promising option for a new generation of high temperature solar thermal concentrating plants. Improved models have been developed [6] and validated by on-sun experiments at pilot scale [7].

Direct absorption systems using particles are very attractive because no window is necessary and they accept very high solar flux density (of the order of 1 MW/m^2), but from the engineering point of view, particle flow stability is difficult to control and convection losses may be high. Indirect absorption solid particle receivers tolerate lower flux density (in the range 200-400 kW/m^2) but they offer a better control of particle circulation within the receiver and a possible management of operating pressure and atmosphere composition. Various options are possible, for example, an annular fluidized bed reactor has been studied [8], a cyclone reactor for biomass conversion has been considered [9] and CNRS developed a “Sand heater loop” using sand particles as HTF [10]. It combined a solar rotary kiln that delivered hot sand to a heat storage / heat recovery sub-system consisting in a hot and a cold heat storage bin and in a multistage fluidized heat exchanger.

One of the main issues for high power solar concentrating system using particles as HTF is the particle mass flow rate that may be flowed inside the solar receiver. In industry, circulating fluidized bed is well-developed at large scale in oil refineries and in combustion plants. For example, in FCC (Fluid Catalytic Cracking) process in petroleum refineries, solid catalytic flow rate as high as 2000 t/h is typical in a single reactor. Generally, the reactor (riser) operates at high gas velocity (several m/s) and dilute solid-gas flows (solid fraction less than 5%) in such systems. Consequently, circulating fluidized bed requires high mechanical energy consumption for compression, leads to poor wall-to-particles heat transfer coefficient. Moreover, the particles high velocities provoke tube erosion and solid particle attrition.

We proposed a new concept; it uses dense suspension of small size solid particles and was patented [11]. This innovation is currently developed in the frame of both a National and a European project (FP7 EC project CSP2, http://www.csp2-project.eu). The dense suspension of particles receiver (DSPR) consists in creating the upward circulation of a dense suspension of particles (solid fraction in the range 30%-40%) in vertical absorbing tubes submitted to concentrated solar energy. The suspension acts as a heat transfer fluid with a heat capacity similar to a liquid HTF but with no temperature limitation but the working temperature limit of the receiver tube. Suspension temperatures up to 750°C are expected for metallic tubes, thus opening new opportunities for high efficiency thermodynamic cycles such as supercritical steam and carbon dioxide [12].

This paper presents experimental results that were obtained during on-sun testing with CNRS solar facility of a single tube DSPR at low temperature (outlet temperature less than 300°C). After explaining the system principle, the experimental setup and operating conditions are presented. Unprocessed test results dealing with temperature distribution and elevation during experiments are presented, and then wall-to-suspension heat transfer coefficients are derived and analysed as a function of the system pertinent parameters. Future developments are finally discussed.

Nomenclature

Latin symbols

A	internal surface area of the receiver tube (m^2)
$C_{p,p}$	solid heat capacity ($J.kg^{-1}K^{-1}$)
d_{32}	Sauter mean diameter (μm)
h	wall-to-suspension heat transfer coefficient ($W/m^2.K$)
$h_{chamber}$	suspension level in the chamber (m)
h_{tube}	suspension level in the tube (m)
$L_{exposed}$	length of the tube exposed to solar radiation (m)
P_{atm}	atmospheric pressure (Pa)
$P_{chamber}$	freeboard pressure (Pa)
F_p	solid mass-flow rate ($kg.s^{-1}$)
r	tube radius (m)
S	tube cross-section area (m^2)
t	time (s)
T_p	solid temperature (K)
T_w^{ext}	tube wall external temperature (K)
T_w^{int}	tube wall internal temperature (K)
U_g	gas superficial velocity ($m.s^{-1}$)
U_{mb}	minimum bubbling velocity ($m.s^{-1}$)
U_{mf}	minimum fluidization velocity ($m.s^{-1}$)
U_p	particles average vertical velocity in the tube ($m.s^{-1}$)

Greek symbols

α_p	particle volume fraction
ε	suspension voidage
ΔP_{motor}	driving pressure of the flow (Pa)
ΔP_{static}	hydrostatic pressure of the suspension (Pa)
$\Delta P/L$	linear pressure drop ($Pa.m^{-1}$)
ΔT_{lm}	logarithmic-mean temperature difference
μ_g	gas dynamic viscosity ($N.s.m^{-2}$)
ρ_g	gas density ($kg.m^{-3}$)
ρ_p	solid density ($kg.m^{-3}$)
τ	average particle passage time through the radiation-exposed part of the tube (s)

2. Principles for circulating a dense suspension of particles in a solar receiver

2.1. Fluidization regimes

In order to achieve the dense suspension state, the superficial velocity of the gas injected at the fluidization plate (fluidization velocity), must be carefully chosen because it sets the fluidization regime:

- When the gas superficial velocity is less than the minimum fluidization velocity, the solid behaves as a porous medium, and the linear pressure drop follows Ergun's law. The drag increases with the gas velocity and starts

counteracting the gravity, causing the bed volume expansion as particles move away from each other. This state is called fixed bed.

- Ergun's law, which is semi-empirical, expresses the linear pressure drop ($\Delta P/L$) as a function of the porous medium voidage (ε), the particle volume fraction (α_p=1- ε), the gas superficial velocity (U_g), density (ρ_g) and dynamic viscosity (μ_g), and of the particle Sauter mean diameter (d_{32}: mean diameter with the same ratio of volume to surface area),

$$\Delta P/L = 150\frac{{\alpha_p}^2}{\varepsilon^3}\frac{\mu_g U_g}{{d_{32}}^2} + 1.75\ \frac{(1-\varepsilon)}{\varepsilon^3}\frac{\rho_g {U_g}^2}{d_{32}} \quad (1)$$

The first part of the equation corresponds to the energy losses due to viscosity, and the second part to the energy losses due to turbulence.

- At the fluidization onset, the linear pressure drop becomes equal to the suspension apparent volumetric weight,

$$\Delta P/L = \left(\alpha_p\rho_s + \varepsilon\rho_g\right)g - \rho_g g = \alpha_p\left(\rho_s - \rho_g\right)g \quad (2)$$

where ρ_s is the solid density and g the gravity acceleration.

- When the gas superficial velocity is comprised between the minimum fluidization velocity (U_{mf}) and the minimum bubbling velocity (U_{mb}), the fluidized bed is homogenous. When reaching U_{mb}, the fluidization becomes heterogeneous with gas bubbles almost void of particles whose passing creates an important particle radial agitation. The agitation being favourable to the wall-to-suspension heat transfer, this regime is chosen for operation.

2.2. Suspension circulation

Once the dense suspension is obtained, its upward circulation must be created in the tube plunging into it. This requires overpressure in the chamber freeboard ($P_{chamber}$), which is obtained by setting a regulation valve at the gas outlet. The pressure at the vertical tube outlet is the atmospheric pressure (P_{atm}). The flow driving force (ΔP_{motor}) is the difference between the two pressures above. The hydrostatic pressure of the suspension (ΔP_{static}), which is the sum of the gas pressure drop across the bed and the gas hydrostatic pressure, maintains the balance with ΔP_{motor}, thus raising the bed level in the tube (h_{tube}),

$$\Delta P_{static} = \left(\Delta P/L + \rho_g g\right)(h_{tube} - h_{chamber}) = \left(\alpha_p\rho_s + \varepsilon\rho_g\right)g(h_{tube} - h_{chamber}) \quad (3)$$

with h_{tube} and $h_{chamber}$ the suspension levels in the tube and in the chamber.

When the suspension hydrostatic pressure in the tube becomes equal to ΔP_{motor}, the level stabilizes. A continuous flow is established by setting the regulation valve so that ΔP_{motor} is higher than the hydrostatic pressure obtained when the suspension level reaches the tube outlet. The flow increases with the pressure difference ΔP_{motor} - ΔP_{static}. Moreover, it is necessary to inject a secondary gas flow into the tube (aeration) at a short distance from its bottom. It helps stabilizing the solid flow that would otherwise be blocked by the suspension subsidence.

2.3. Solid flow control

The solid flow is controlled by two parameters: the pressure into the fluidization chamber (due to the regulation valve) and the aeration flow rate. The pressure increase induces a solid mass-flow rate increase, while the suspension voidage remains unchanged. The aeration, in addition to its stabilizing role, is used to control the suspension density. It is possible to increase the suspension voidage by injecting a gas flow rate higher than the minimum required for stabilization. But the hydrostatic pressure lowering is another consequence. By maintaining the chamber pressure constant, it increases the solid mass-flow rate. To summarize, raising the chamber pressure increases the solid flow rate, and increasing the aeration flow rate decreases the suspension density while increasing the solid flow rate.

3. Experimental setup and procedure

The general principle of the solar rig using a DSP as the heat transfer fluid and that was set at the focus of the CNRS 1 MW solar furnace is schemed in Fig. 1. In this lab-scale experimental setup, the solar absorber is a single opaque metallic tube ① that is located inside a cylindrical cavity dug in a receiver made of alkaline-earth silicate (Insulfrax®), and submitted to the concentrated solar radiation. The receiver average wall thickness is 0.28 m, the cavity is 0.20 m in diameter, and it is irradiated through a 0.10m x 0.50m slot set at the focus plane, with aperture angle 126°. The whole experimental setup is set behind a water-cooled aluminum shield that protects both personnel and equipment from high solar flux when running solar experiments.

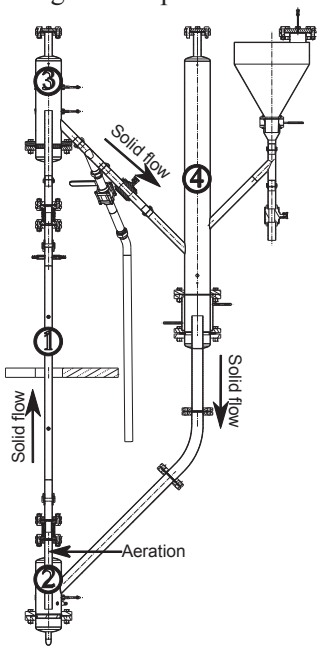

Fig. 1. Schematic view of the solar loop. ①solar absorber metallic tube; ② particle suspension dispenser; ③ receiving fluidized bed; ④ suspension return.

The DSP is composed of about 30%-40%% of particles and 70%-60%% of air, it moves upward vertically in the tube constituting the solar absorber by the pressure difference imposed between the particle suspension dispenser (② at the tube bottom) and the receiving fluidized bed (③ at the tube top). This 42.4 mm o.d. AISI 310S stainless steel tube (wall thickness 3.2 mm) is submitted to the concentrated solar radiation.

The solid circulating in the suspension is silicon carbide, mainly because of its thermal properties (high sintering temperature, high heat capacity), availability and rather low cost. The chosen particles mean diameter (Sauter mean diameter = 63.9 μm) permits a good fluidization quality with almost no bubbles, for very low air fluidization velocities (U_{mf} = 5 mm/s at 20°C) since they belong to Geldart's Group A of particles [13]. Table 1 lists the physical properties of the solid.

Table 1 Physical properties of SiC particles

$\rho C_{p,p}$ [kJ/m3.K]	$T_{sintering}$ [°C]	λ [W/m.K]	ε_{mb}	ε_{mf}	U_{mf} [10-3 m.s-1]	U_{mb} [10-3 m.s-1]	d_{32} [μm]
3000	1620	18	0.59	0.57	5.5	6.6	63.9

4. Measurement results

The system testing was carried on under various ranges of the operating parameters, which are the solid superficial mass-flow rate (F_p/S), the aeration at the base of the tube, and the solar flux density at the receiver entrance. Since the system is operated in batch, the solid mass-flow rate determines the duration of each experiment, which ranged between twenty and forty minutes. The slip velocity between the gas and solid at the tube inlet is close to the minimum fluidization velocity, regardless of the operating conditions. This was put into evidence by a helium tracking technique set on a cold mock-up [14]. Since the solid mass-flow rate is known, the gas superficial velocity at the tube inlet can be obtained. The solar flux density was measured at the receiver entrance and not on the absorbing tube. Actually its variations were not sufficient to change significantly the results. Table 2 summarizes the considered ranges of operating parameters.

Table 2 Ranges of operating parameters

F_p/S	U_g tube inlet	Aeration	Solar flux density
[$kg.m^{-2}.s^{-1}$]	[10^{-3} $m.s^{-1}$]	[$sm^3.s^{-1}.m^{-2}$]	[$kW.m^{-2}$]
7.4 - 24.6	8.8 - 13.2	0.011 - 0.109	200 - 245

Logically, the various operating parameters' values influenced the solid temperature at the inlet and at the outlet of the irradiated cavity ($T_{p,i}$ and $T_{p,o}$), the wall temperature at the inlet, in the middle and at the outlet of the irradiated cavity ($T_{w,i}^{ext}$, $T_{w,m}^{ext}$ and $T_{w,o}^{ext}$), the pressure drop along the tube ($\Delta P/L$) and the power transmitted to the suspension (Φ). Table 3 lists the ranges of experimental results.

Table 3 Ranges of experimental results

$T_{p,i}$	$T_{p,o}$	$T_{w,i}^{ext}$	$T_{w,m}^{ext}$	$T_{w,o}^{ext}$	$\Delta P/L$	Φ
[°C]	[°C]	[°C]	[°C]	[°C]	[Pa/m]	[W]
41 - 248	164 - 317	144 - 344	204 - 378	229 - 379	8500 - 11200	443 - 2724

Let focus on the temperatures measured at different locations on the absorber tube. As detailed before, the tube wall outside temperature is measured by several K thermocouples soldered on the tube rear. Fig. 2(a) displays the values given by the 3 thermocouples set at the height middle of the tube (both sides and the rear). There exists a significant temperature difference between their indications, similarly to the differences measured at the lower and upper parts of the tube inside the cavity. Two sheathed thermocouples set downstream the receiver cavity also give different solid outlet temperature values; see Fig. 2(b). The same phenomenon is noticed at the cavity inlet. However, this suspension heterogeneity disappears when the solid exits the sun-irradiated cavity. Therefore, we used the average of all measurements made at one position as the mean temperature value in the heat transfer coefficient analysis.

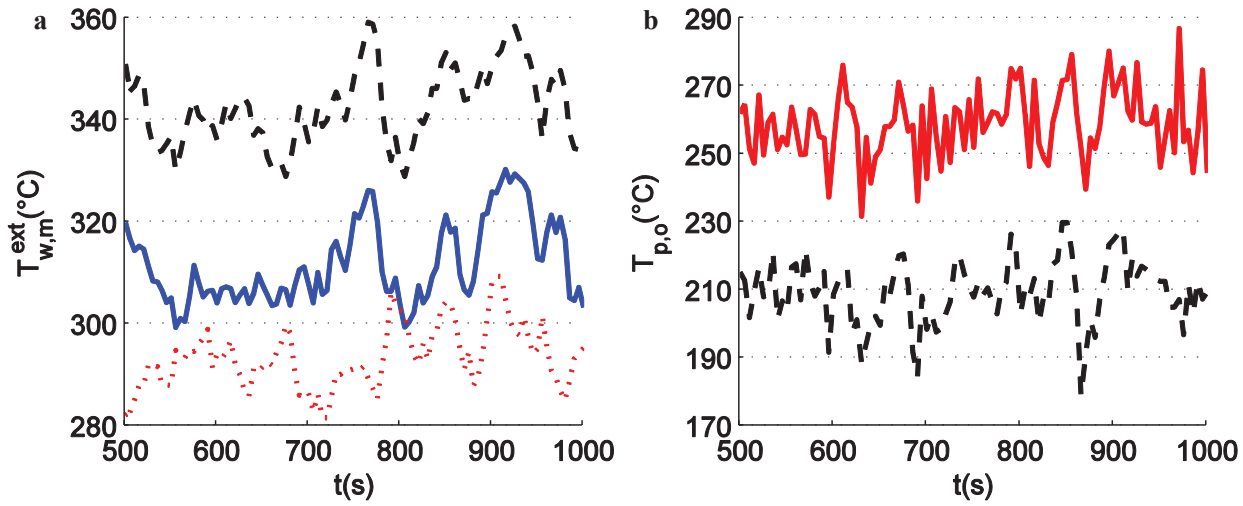

Fig. 2 (a) Wall external temperatures in the middle of the tube (left ····· , back ── , right ----) ; (b) Solid temperatures at the outlet of the receiver cavity (5 mm from the wall ----, center of the tube ──)

Fig. 3 displays the temporal profile of the solid temperature at the inlet and outlet of the irradiated cavity, and their difference. This plot is gives an idea of the system response time to changes in irradiation or circulation conditions. First, there is no solid circulation. The suspension level in the tube is stabilized. Initial time t = 0 s is the moment when receiver cavity irradiation starts. During the first 4 minutes, the system heats up. Then at t = 240 s, the valve pressure setting is increased and the solid begins to circulate. Therefore, a temperature difference is established between the inlet and the outlet. It takes approximately 3 minutes to stabilize the temperature difference around 65°C. In our experiments, the system was able to change from the cold static state (no solid circulation, no solar irradiation) to a stable operating state in about 6 minutes. While in operation, it takes less than 30 seconds to go from a stable state to another one when changing the settings. So we can say that this system has a short reaction time, which is very useful because of the solar irradiation variations.

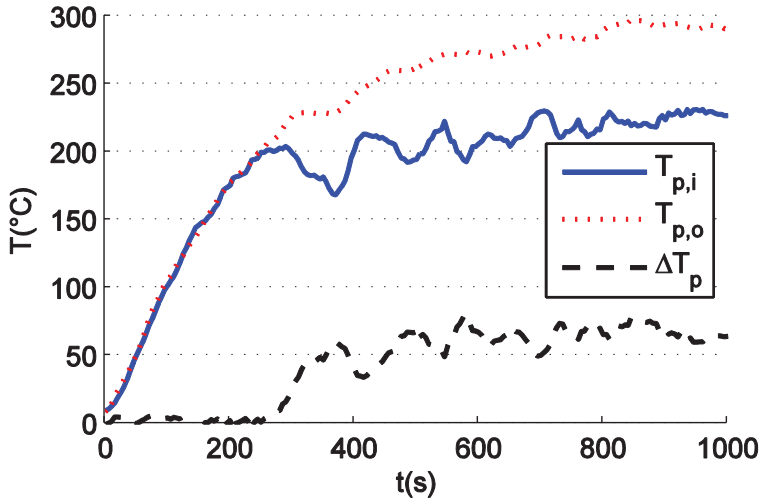

Fig. 3 Solid temperature as a function of time in the irradiated cavity (Operating conditions: Average solid superficial mass-flow rate = 12.28 kg/m^2.s; Aeration = 0.109 sm^3/m^2.s; Solar flux density = 223 kW/m^2)

5. Heat transfer results and analysis

5.1. Heat transfer coefficient calculation

The main objective of the first series of experiments was to calculate the heat transfer coefficient between the dense suspension and the tube wall, and to determine the parameters affecting it.

The air heat capacity is neglected in comparison to that of the solid ($C_{p,s}$). Therefore, the power transmitted to the suspension inside the receiver tube is

$$\Phi = F_p \int_{T_{p,i}}^{T_{p,o}} C_{p,p} dT \approx F_p . C_{p,p} \left(\frac{T_{p,i}+T_{p,o}}{2}\right)\left(T_{p,o} - T_{p,i}\right) \quad (4)$$

where F_p is the solid mass-flow rate and T_s the solid temperature (index o and i for outlet and inlet respectively).

The wall internal temperature T_w^{int} is calculated from the wall external temperature, the steel conductivity and the heat flux received by the suspension while going up the receiver tube. Since we do not have data on the distribution of the heat flux passing through the tube wall, it is supposed to be uniform on all the tube.

Typical temperature vs. time profiles for the external wall and the solid along the tube are similar to the temperature profiles in a counter-flow heat exchanger. This justifies the calculation of a logarithmic-mean temperature difference (ΔT_{lm}) is calculated from the solid and internal wall temperatures,

$$\Delta T_{lm} = \left[T_w^{int} - T_p\right]_o^i \Big/ ln\left(\frac{T_{w,i}^{int} - T_{p,i}}{T_{w,o}^{int} - T_{p,o}}\right) \quad (5)$$

With A the internal surface area of the tube receiver, the heat transfer coefficient h is then deduced from the formula

$$\Phi = h . A . \Delta T_{lm} \quad (6)$$

5.2. Analysis of pertinent parameters for wall-to-suspension heat transfer

The power transferred to the suspension can be defined in two different ways: as a function of the heat transfer coefficient and of the ΔT_{lm}, or as a function of the solid mass-flow rate and of temperatures. The solid mass-flow rate itself depends on the average particle volume fraction α_p and on their average vertical velocity U_p or the average passage time through the irradiated part of the tube τ ($U_p = L_{tube}/\tau$). This allows writing:

$$h . \Delta T_{lm} = \frac{\rho_p . r}{2} . \alpha_p . \frac{1}{\tau} . C_{p,p} \left(\frac{T_{p,i}+T_{p,o}}{2}\right)\left(T_{p,o} - T_{p,i}\right) = \frac{\rho_p . r}{2 . L_{exposed}} . \alpha_p . U_{p,z} . C_{p,p} \left(\frac{T_{p,i}+T_{p,o}}{2}\right)\left(T_{p,o} - T_{p,i}\right) \quad (7)$$

where r is the tube radius, L_{tube} the length of the irradiated part of the tube and ρ_s the particle density.

Consequently, we studied the influence of these pertinent parameters. Fig. 4 shows the variations of the heat transfer coefficient as a function of the particle average vertical velocity when the particle volume fraction is comprised between 0.29 and 0.32. The lowest heat transfer coefficient is 164 $W.m^{-2}.K^{-1}$. It was obtained at 10.1 $mm.s^{-1}$ mean particle vertical velocity, and 9.01 $kg.m^{-2}.s^{-1}$ solid superficial mass-flow rate. The highest heat transfer coefficient is 454 $W.m^{-2}.K^{-1}$. It was obtained at 26.4 $mm.s^{-1}$ mean particle vertical velocity, and 24 $kg.m^{-2}.s^{-1}$ solid superficial mass-flow rate. The data were interpolated as a linear function of the mean particle velocity: $h_{linear}(U_p) = a.U_p + b$, with a = 17.532 $J.m^{-3}.K^{-1}$ and b = 14.9529 $W.m^{-2}.K^{-1}$. The faster the particles movement, the higher the heat transfer coefficient; this comes directly from the much higher particle mixing obtained when the particles circulate faster, which increases the particles exchange between the wall and the tube center. As a last comment, it should be noticed in the plot that the higher the range of particle volume fraction, the higher the heat transfer coefficient.

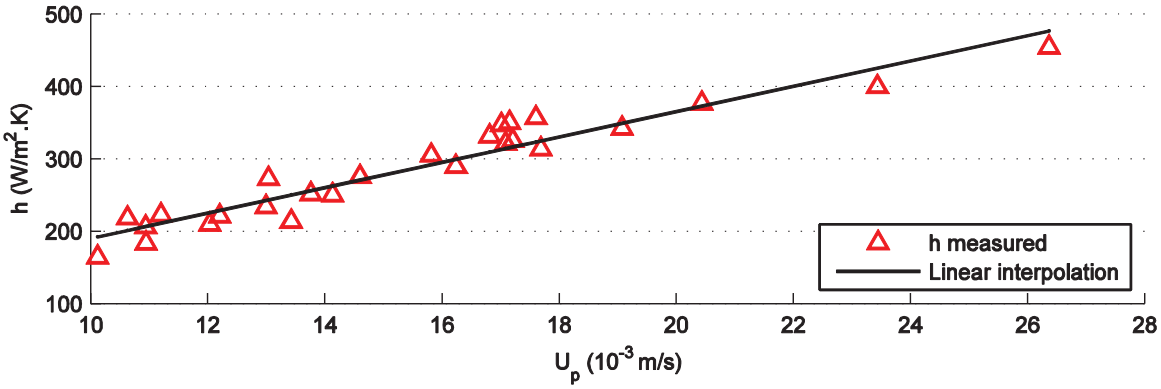

Fig. 4 Average heat transfer coefficient as a function of the average particle vertical velocity for the range of particle volume fraction 0.29-0.32

Fig. 5 features the heat transfer coefficient as a function of the particle volume fraction when the passage time through the solar-irradiated part of the tube ranged between 31s and 36 s. The lowest heat transfer coefficient is 149 $W.m^{-2}.K^{-1}$. It was obtained at 0.26 mean particle volume fraction and 11.3 $kg.m^{-2}.s^{-1}$ solid superficial mass-flow rate. The highest heat transfer coefficient is 374 $W.m^{-2}.K^{-1}$. It was obtained at 0.336 and 16.65 $kg.m^{-2}.s^{-1}$ mean particle volume fraction and solid superficial mass-flow rate respectively. The data were interpolated as a linear function of the mean particle volume fraction: $h_{linear}(\alpha_p) = c.\alpha_p + d$, with c = 2799.3 $W.m^{-2}.K^{-1}$and d = -566.32 $W.m^{-2}.K^{-1}$. The higher the particle volume fraction, the higher the heat transfer coefficient; the reason is that the contact area between the particles and the tube internal surface is greater when the particles occupy a greater volume fraction.

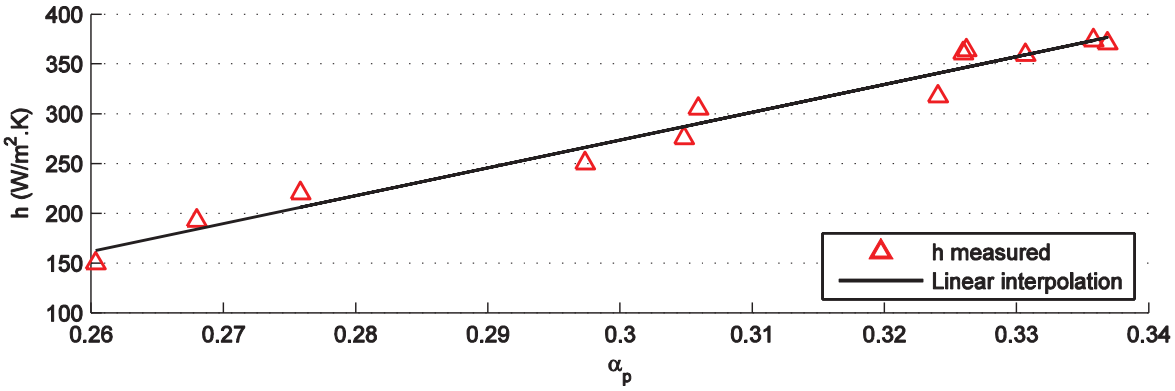

Fig. 5 Average heat transfer coefficient as a function of particle volume fraction for the range of passage time 31-36s

6. Conclusion and future work

The aim of the study was to run a first series of on-sun experiments involving a new type of solar receiver that uses a dense suspension of solid particles (DSP) circulating upward in an opaque tube exposed to the concentrated solar flux.

Contrarily to circulating fluidized beds (CFB), DSP flows operate at low gas velocity and large solid fraction. For the group A particles, typical air velocity and mean solid fraction in CFB are of the order of 1 m/s and less than 1% respectively; these values are typically 10 mm/s and 35% in DSP.

It was shown that this innovative process leads to heat transfer coefficients up to 500 $W/m^2.K$ in the considered conditions, with particle mean velocities always less than 2.5 cm/s. We found that the particle velocity and the particle volume fraction are the main parameters influencing the heat transfer coefficient. The higher the particle

velocity, the higher the heat transfer coefficient, because the particle agitation increases, thus improving the particle movement and the exchange between the wall and the tube center. In addition, the higher the particle volume fraction, the higher the heat transfer coefficient, since when particles occupy a greater volume, the contact area with the tube wall is larger.

On the basis of 400 W/m².K mean heat transfer coefficient obtained at low temperature (about 250°C), one can expect higher heat transfer coefficient at 800°C since it increases with temperature due to the increase of particle and gas thermophysical properties (thermal conductivity for air and heat capacity for SiC) and to radiation contribution [15]. Thus DSP extends drastically the operating temperature range of solar heat transfer fluids, limited to about 560°C nowadays, while keeping both advantages of being HTF and storage medium. Suspension temperatures up to 750°C are expected for metallic tubes, thus opening new opportunities for high efficiency thermodynamic cycles such as supercritical steam and supercritical carbon dioxide. Using ceramic tubes may extend the operating temperature up to more than 1000°C, i.e. Brayton and combined cycles. Operation with incident solar flux density of about 300-400 kW/m^2 can be anticipated, since heat transfer coefficient is about 4 times less than that of molten salts. This lower acceptable nominal solar flux is compensated by higher operating temperature and no heating requirement against freezing risk.

Next step of this study will be operating DSP in the temperature range 500-700°C.

Acknowledgements

This work was funded by French CNRS (Energy Program) and by European Commission, FP7 (CSP2 Project, Grant Agreement 82932).

References

[1] Flamant G., 1982. Theoretical and experimental study of radiant heat transfer in a solar fluidized-bed receiver. AIChE Journal 28, 529-535.

[2] Martin J., Vitko J., 1982. ASCUAS: a solar central receiver utilizing a solid thermal carrier. Sandia National Laboratories, Report SAND82-8203.

[3] Flamant G., Hernandez D., Bonet C., Traverse J-P, 1980. Experimental aspects of the thermochemical conversion of solar energy; Decarbonation of $CaCO_3$. Solar Energy, 24, 385-395.

[4] Falcone P.K., Noring J.E., Hruby J.M., 1985. Assessment of a solid particle receiver for a high temperature solar central receiver system. Sandia National Laboratories, Report SAND85-8208. [5] Evans G., Houf W., Grief R., Crowe C., 1987. Gas-Particle Flow Within a High Temperature Solar Cavity Receiver Including Radiation Heat Transfer. ASME Journal of Solar Energy Engineering. 109, 134-142.

[6] Siegel N, Ho C.K, Khalsaz S.S., Kolb G.J., 2010. Development and Evaluation of a Prototype Solid Particle Receiver: On-Sun Testing and Model Validation. ASME Journal of Solar Energy Engineering 132, 021008.

[7] Chen H., Chen Y., Hsieh H.T., Siegel N., 2007. CFD Modeling of Gas Particle Flow within a Solid Particle Solar Receiver. ASME Journal of Solar Energy Engineering, 129, 160-170.

[8] Badie J-M., Bonet C., Faure M., Flamant G., Foro R., Hernandez D., 1980. Decarbonation of calcite and phosphate rock in solar chemical reactors. Chemical Engineering Science, 35, 413-420.

[9] Lédé J., Verzaro F., Antoine B., Villermaux J., 1986. Flash pyrolysis of wood in a cyclone reactor. Chemical Engineering and Processing: Process Intensification 20, 309–317.

[10] Bataille D., Laguerie C., Royere C, Gauthier D., 1989. Gas-solid heat exchangers with multistage fluidized beds in the range of average and high temperature. Entropie 25, 113-126.

[11] Flamant G., Hemati M., French Patent N° 1058565, 20 October 2010. PCT extension, 26 April 2012, N° WO 2012/052661 A2.

[12] Pitz-Paal R., Amin A, Bettzuge M.O., Eames P., Flamant G., Fabrizzi F., Homes J., Kribus A., Van der Lan H., Lopez C., Garcia Novo F., Papagiannakopoulos P., Pihl E., Smith P., Wagner H-J., 2012. Concentrating Solar Power in Europe, the Middle East and North Africa: A Review of Development Issues and Potential to 2050. ASME Journal of Solar Energy Engineering 134, 024501.

[13] Geldart D., 1973. Types of gas fluidization. Powder Technology 7, 285-292.

[14] Boissière B., Ansart R. , Hemati M., Gauthier D., Flamant G., 2012. 7ème Colloque Science et Technologie des Poudres, STP2012, Toulouse, FRANCE, 4-6 Juillet 2012.

[15] Flamant G. and Ménigault T., 1987. Combined wall-to-fluidized bed heat transfer. Bubbles and emulsion contributions at high temperature. International Journal of Heat and Mass Transfer 30, 1803-1812.